Melting tungsten nanoparticles: a molecular dynamics study

2008 J. Phys. D: Appl. Phys. 41 185406

(http://iopscience.iop.org/0022-3727/41/18/185406)

IOP PUBLISHING JOURNAL OF PHYSICS D: APPLIED PHYSICS

J. Phys. D: Appl. Phys. **41** (2008) 185406 (7pp) doi:10.1088/0022-3727/41/18/185406

Melting tungsten nanoparticles: a molecular dynamics study

Amitava Moitra[1,2], Sungho Kim[1,2], Jeff Houze[1,2], Bohumir Jelinek[1,2], Seong-Gon Kim[1,2], Seong-Jin Park[2,3], Randall M German[2,3] and Mark F Horstemeyer[2,3]

[1] Department of Physics and Astronomy, Mississippi State University, Mississippi State, MS 39762, USA
[2] Center for Advanced Vehicular Systems, Mississippi State University, Mississippi State, MS 39762, USA
[3] Department of Mechanical Engineering, Mississippi State University, Mississippi State, MS 39762, USA

Received 17 December 2007, in final form 20 June 2008
Published 28 August 2008
Online at stacks.iop.org/JPhysD/41/185406

Abstract

We report a molecular dynamics simulation of melting of tungsten (W) nanoparticles. The modified embedded atom method interatomic potentials are used to describe the interaction between tungsten atoms. The melting temperature of unsupported tungsten nanoparticles of different sizes are found to decrease as the size of the particles decreases. The melting temperature obtained in this study is approximately a decreasing function of inverse radius, in good agreement with the predictions of thermodynamic models. We also observed that the melting of a W nanoparticle is preceded by the premelting of its outer skin at a temperature lower than its melting temperature.

(Some figures in this article are in colour only in the electronic version)

1. Introduction

Tungsten, along with its alloys and compounds, occupies a unique position in materials science. The material properties that make tungsten attractive to the metals industry are high density, hardness, melting temperature, elastic modulus and conductivity in conjunction with the low thermal expansion. The combination of these unique properties explains the diverse applications of tungsten ranging from home lighting to thermonuclear fusion firstwall protection [1, 2]. With nanoscale tungsten powders available at a reasonable cost, its usage will increase greatly and a new approach is required to balance the size dependent advantages against the temperature dependent limitations. Therefore, it is of great importance to understand the thermal stability of tungsten nanoparticles for their applications at higher temperatures. It has been seen previously that nanoparticles exhibit a significant decrease in melting temperatures compared with infinite bulk solids [3]. This is related to the fact that the liquid–vapour interface energy is generally lower than the average solid–vapour interface energy [4]. Based on thermodynamics, a phenomenological relation between the melting temperature and particle size has been obtained: the melting temperature of a nanoparticle decreases inversely proportionally to the particle diameter [3–5]. It is also known that premelting, the phenomenon where the surface atoms of nanoparticles lose their solid ordering and hence melt prior to complete melting of the whole particle [5–10], plays an important role in understanding the melting of nanoparticles. On the other hand, the Hall–Petch effect—the hardness increases in proportion to the inverse square-root of grain size [11, 12]—suggests that significant opportunities exist if nanoscale powders could be consolidated to full densities with minimized coarsening. Hence, knowledge of accurate melting temperature for different particle size plays an important role for the advancement of present engineering and technological growth.

Molecular dynamics simulations offer an effective tool to study the melting and coalescence of nanoparticles [13, 14]. These atomistic simulations require accurate atomic interaction potentials to compute the total energy of the system. First-principles calculations can provide the most reliable interatomic potentials. However, realistic simulations of the melting of nanoparticles often require a number of atoms that render these methods impractical: they either require too much computer memory or take too long to be completed in a reasonable amount of time. One alternative is to use empirical

or semi-empirical interaction potentials that can be evaluated efficiently. In this study, we use the modified embedded atom method (MEAM) originally proposed by Baskes *et al* [15, 16]. MEAM was the first semi-empirical atomic potential using a single formalism for fcc, bcc, hcp, diamond-structured materials and even gaseous elements, in good agreement with experiments or first-principles calculations [16, 17]. The MEAM is an extension of the embedded atom method (EAM) [18–20] to include angular forces. Cherne *et al* made a careful comparison of MEAM and EAM calculations in a liquid nickel system [21].

Atomistic simulations of a wide range of elements and alloys have been performed using the MEAM potentials. A realistic shear behaviour for silicon was first obtained using the MEAM by Baskes *et al* [15]. The MEAM was also applied to various single elements [16] and to silicon–nickel alloys and interfaces [22]. Gall *et al* used the MEAM to model the tensile debonding of an aluminium–silicon interface [23]. Lee and Baskes extended the MEAM to include the second nearest-neighbour interactions [24]. A new analytic modified embedded atom method (AMEAM) many-body potential was also proposed and applied to several hcp metals, including Mg [25, 26]. For the Mg–Al alloy system, a set of EAM potentials has been developed using the 'force matching' method by Liu *et al* [27]. Recently, a new set of MEAM potentials for Mg–Al alloy system was developed by Jelinek *et al* [28]. These new potentials show a significant improvement over the previously published potentials, especially for the surface formation, stacking faults and point defect formation energies.

The paper is organized in the following manner. In section 2, we give a brief review of the MEAM. In section 3, the procedure for melting simulation is presented. MD simulation results are presented and discussed in section 4. Finally, in section 5, we summarize our findings.

2. MEAM theory

The total energy E of a system of atoms in the MEAM [29] is approximated as the sum of the atomic energies

$$E = \sum_i E_i. \tag{1}$$

The energy of atom i consists of the embedding energy and the pair potential terms:

$$E_i = F_i(\bar{\rho}_i) + \frac{1}{2}\sum_{j\neq i}\phi_{ij}(r_{ij}). \tag{2}$$

F_i is the embedding function of atom i, $\bar{\rho}_i$ is the background electron density at the site of atom i and $\phi_{ij}(r_{ij})$ is the pair potential between atoms i and j separated by a distance r_{ij}. The embedding energy $F_i(\bar{\rho}_i)$ represents the energy cost to insert atom i at a site where the background electron density is $\bar{\rho}_i$. The embedding energy is given in the form

$$F_i(\bar{\rho}_i) = A_i E_i^0 \bar{\rho}_i \ln(\bar{\rho}_i), \tag{3}$$

where the sublimation energy E_i^0 and parameter A_i depend on the element type of atom i. The background electron density $\bar{\rho}_i$ is given by

$$\bar{\rho}_i = \frac{\rho_i^{(0)}}{\rho_i^0} G(\Gamma_i), \tag{4}$$

where

$$\Gamma_i = \sum_{k=1}^{3} \bar{t}_i^{(k)} \left(\frac{\rho_i^{(k)}}{\rho_i^{(0)}}\right)^2 \tag{5}$$

and

$$G(\Gamma) = \sqrt{1+\Gamma}. \tag{6}$$

The zeroth and higher order densities, $\rho_i^{(0)}$, $\rho_i^{(1)}$, $\rho_i^{(2)}$ and $\rho_i^{(3)}$ are given in equation (9). The composition-dependent electron density scaling ρ_i^0 is given by

$$\rho_i^0 = \rho_{i0} Z_{i0} G(\Gamma_i^{\text{ref}}), \tag{7}$$

where ρ_{i0} is an element-dependent density scaling, Z_{i0} is the first nearest-neighbour coordination of the reference system and Γ_i^{ref} is given by

$$\Gamma_i^{\text{ref}} = \frac{1}{Z_{i0}^2}\sum_{k=1}^{3} \bar{t}_i^{(k)} s_i^{(k)}, \tag{8}$$

where $s_i^{(k)}$ is the shape factor that depends on the reference structure for atom i. Shape factors for various structures are specified in the work of Baskes [16]. The partial electron densities are given by

$$\rho_i^{(0)} = \sum_{j\neq i} \rho_j^{a(0)} S_{ij}, \tag{9a}$$

$$(\rho_i^{(1)})^2 = \sum_{\alpha}\left[\sum_{j\neq i}\rho_j^{a(1)}\frac{r_{ij\alpha}}{r_{ij}}S_{ij}\right]^2, \tag{9b}$$

$$(\rho_i^{(2)})^2 = \sum_{\alpha,\beta}\left[\sum_{j\neq i}\rho_j^{a(2)}\frac{r_{ij\alpha}r_{ij\beta}}{r_{ij}^2}S_{ij}\right]^2 - \frac{1}{3}\left[\sum_{j\neq i}\rho_j^{a(2)}S_{ij}\right]^2, \tag{9c}$$

$$(\rho_i^{(3)})^2 = \sum_{\alpha,\beta,\gamma}\left[\sum_{j\neq i}\rho_j^{a(3)}\frac{r_{ij\alpha}r_{ij\beta}r_{ij\gamma}}{r_{ij}^3}S_{ij}\right]^2 - \frac{3}{5}\sum_{\alpha}\left[\sum_{j\neq i}\rho_j^{a(3)}\frac{r_{ij\alpha}}{r_{ij}}S_{ij}\right]^2, \tag{9d}$$

where $r_{ij\alpha}$ is the α component of the displacement vector from atom i to atom j. S_{ij} is the screening function between atoms i and j and is defined in equations (16*a*)–(16*e*). The atomic electron densities are computed as

$$\rho_i^{a(k)}(r_{ij}) = \rho_{i0}\exp\left[-\beta_i^{(k)}\left(\frac{r_{ij}}{r_i^0}-1\right)\right], \tag{10}$$

where r_i^0 is the nearest-neighbour distance in the single-element reference structure and $\beta_i^{(k)}$ is an element-dependent parameter. Finally, the average weighting factors are given by

$$\bar{t}_i^{(k)} = \frac{1}{\rho_i^{(0)}}\sum_{j\neq i} t_j^{(k)} \rho_j^{a(0)} S_{ij}, \tag{11}$$

where $t_j^{(k)}$ is an element-dependent parameter.

The pair potential is given by

$$\phi_{ij}(r_{ij}) = \bar{\phi}_{ij}(r_{ij}) S_{ij}, \tag{12}$$

$$\bar{\phi}_{ij}(r_{ij}) = \frac{1}{Z_{ij}}\left[2E^u_{ij}(r_{ij}) - F_i\left(\frac{Z_{ij}\rho^{(0)}_j(r_{ij})}{Z_i\rho^0_i}\right) - F_j\left(\frac{Z_{ij}\rho^{(0)}_i(r_{ij})}{Z_j\rho^0_j}\right)\right], \tag{13}$$

$$E^u_{ij}(r_{ij}) = -E^0_{ij}(1 + a^*_{ij}(r_{ij}))\mathrm{e}^{-a^*_{ij}(r_{ij})}, \tag{14}$$

$$a^*_{ij}(r_{ij}) = \alpha_{ij}\left(\frac{r_{ij}}{r^0_{ij}} - 1\right), \tag{15}$$

where α_{ij} is an element-dependent parameter. The sublimation energy E^0_{ij}, the equilibrium nearest-neighbour distance r^0_{ij} and the number of nearest-neighbours Z_{ij} are obtained from the reference structure.

The screening function S_{ij} is designed so that $S_{ij} = 1$ if atoms i and j are unscreened and within the cutoff radius r_c, and $S_{ij} = 0$ if they are completely screened or outside the cutoff radius. It varies smoothly between 0 and 1 for partial screening. The total screening function is the product of a radial cutoff function and three-body terms involving all other atoms in the system:

$$S_{ij} = \bar{S}_{ij} f_c\left(\frac{r_c - r_{ij}}{\Delta r}\right), \tag{16a}$$

$$\bar{S}_{ij} = \prod_{k\neq i,j} S_{ikj}, \tag{16b}$$

$$S_{ikj} = f_c\left(\frac{C_{ikj} - C_{\min,ikj}}{C_{\max,ikj} - C_{\min,ikj}}\right), \tag{16c}$$

$$C_{ikj} = 1 + 2\frac{r^2_{ij}r^2_{ik} + r^2_{ij}r^2_{jk} - r^4_{ij}}{r^4_{ij} - (r^2_{ik} - r^2_{jk})^2}, \tag{16d}$$

$$f_c(x) = \begin{cases} 1 & x \geqslant 1 \\ [1 - (1-x)^4]^2 & 0 < x < 1 \\ 0 & x \leqslant 0 \end{cases}. \tag{16e}$$

Note that $C_{\min}$ and $C_{\max}$ can be defined separately for each i–j–k triplet, based on their element types. The parameter Δr controls the distance over which the radial cutoff function changes from 1 to 0 near $r = r_c$.

3. Molecular dynamics simulation

3.1. Atomic potential

We use the MEAM potential parameters for tungsten (W) proposed by Baskes [16]. The potential parameters that are used for our simulation of W nanoparticles are listed in table 1. These parameters are obtained by fitting the room temperature elastic properties using bcc as the reference structure. $C_{\max}$ and $C_{\min}$ are chosen to include only the first nearest-neighbour interactions [30].

The physical properties of W computed using the present MEAM parameters are compared with those of DFT calculations, as shown in table 2. All first-principles calculations have been performed using DFT as implemented in the VASP code [33]. Energy calculations and geometry optimizations of various structures were performed using Blöchl's all-electron projector augmented wave (PAW) method [32] as implemented by Kresse and Joubert [33]. For the treatment of electron exchange and correlation, we used the generalized gradient approximation (GGA) using the Perdew–Burke–Ernzerhof scheme [34]. The plane-wave cutoff energy was set to 300 eV in all calculations and the Brillouin zone was sampled using the Monkhorst–Pack scheme [31].

Table 2 shows that the results of DFT calculations and experimental values are reproduced satisfactorily by the present MEAM parameters for W. In particular, we note that the elastic constants are well matched with the experimental values, although the present MEAM parameters show a tendency to underestimate the bulk modulus and the surface energies. As we discuss further in section 4, this shortcoming will cause W nanoparticles to melt at lower temperatures due to premature premelting of surface layers.

Table 1. The MEAM potential parameters for W from [30]. E^0 is the sublimation energy, r^0 is the equilibrium nearest-neighbour distance, A is the scaling factor for the embedding energy, α is the exponential decay factor for the universal energy function, $\beta^{(0-3)}$ are the exponential decay factors for the atomic densities, $t^{(0-3)}$ are the weighting factors for the atomic densities and $C_{\max}$ and $C_{\min}$ are the screening parameters.

E^0 (eV)	r^0 (Å)	A	α	$\beta^{(0)}$	$\beta^{(1)}$	$\beta^{(2)}$
8.66	2.74	0.98	5.63	3.98	1.00	1.00
$\beta^{(3)}$	$t^{(0)}$	$t^{(1)}$	$t^{(2)}$	$t^{(3)}$	$C_{\max}$	$C_{\min}$
1.00	1.00	3.16	8.25	−2.70	2.80	2.00

Table 2. Calculated physical properties of W using the present MEAM parameters in comparison with DFT calculations. B_0 is the bulk modulus (GPa); C_{11}, C_{12}, C_{44} are the elastic constants (GPa); $E_{(100)}$, $E_{(110)}$, $E_{(111)}$ are surface energies of corresponding surfaces (mJ m^{-2}); ΔEs are the structural energy differences (eV/atom).

Parameter	DFT	Expt. [54]	MEAM
B_0	330	314	270
$(C_{11} - C_{12})/2$	190	163	160
C_{44}	280	163	160
$E_{(1\,0\,0)}$	7810		5980
$E_{(1\,1\,0)}$	6390		5660
$E_{(1\,1\,1)}$	7190		5030
$\Delta E_{\mathrm{bcc}\to\mathrm{fcc}}$	0.494		0.325
$\Delta E_{\mathrm{bcc}\to\mathrm{hcp}}$	0.397		2.168

3.2. Simulation procedure

We performed detailed MD simulations of the melting of unsupported spherical bcc W nanoparticles with diameters in the range 2–12 nm (259–56 905 atoms). The surface boundary condition was free and no external pressure was applied. Each nanoparticle was constructed by cutting out atoms within a specified radius from the tungsten bulk in the bcc structure that is the stable phase of W at standard temperature and pressure (STP). We also note that the present MEAM parameters predict

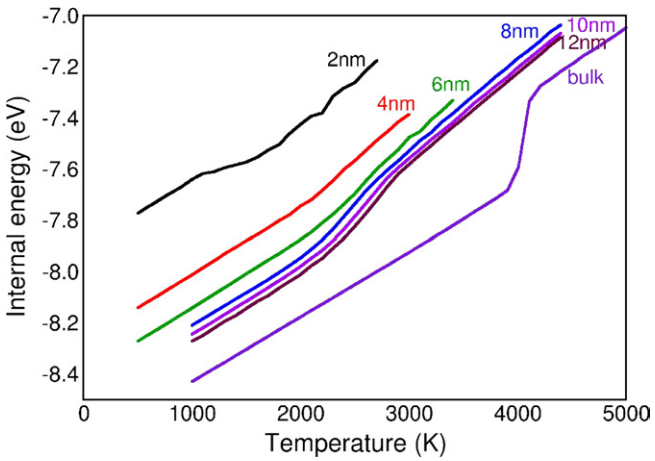

Figure 1. The internal energies per atom of the W nanoparticles with different diameters as a function of temperature. The same data for W bulk are also shown.

the bcc phase to be the most stable structure in these conditions as shown in table 2. Ten different initial configurations for each size of nanoparticles are then obtained by performing MD simulations at the room temperature for 30 000 time steps and saving the atomic configurations at every 3000 time step. We complete the preparation of initial configurations by randomizing the atomic velocities of the nanoparticles according to the Maxwell–Boltzmann distribution at the initial temperature $T_i = 500\,\mathrm{K}$. The equations of motion were integrated using time steps $\Delta t = 4 \times 10^{-15}\,\mathrm{s}$.

We increase the temperature of the heat bath in steps of $\Delta T = 100\,\mathrm{K}$ from the initial temperature $T_i = 500\,\mathrm{K}$ to the final temperature up to $T_f = 4000\,\mathrm{K}$. We run the MD simulations for 50 000 time steps at each temperature. Statistical (time-averaged) data for energetics are collected after the system has adjusted to the new temperature, which is typically after 25 000 time steps following a temperature increase. For the particles of diameters less than 8 nm, 20 000 time steps were used to adjust the particles to each new temperature. The isothermal condition was maintained by using Nosé–Hoover thermostat [35, 36]. Final results are obtained by taking the ensemble average among the 10 different samples for each size.

4. Results and discussion

The most straightforward method to identify the melting of atomistic structures in MD simulations is to monitor the variation of the internal energy with temperature. Figure 1 shows the internal energies per atom of the W nanoparticles with different diameters as a function of temperature. It is seen from figure 1 that each internal energy curve goes from one linear region to another. The overall melting is identified by the 'jump' connecting these two linear regions in the internal energy curve. The height of the jump is a measure of ΔH_m, the amount of heat required for melting, and it decreases as the size of nanoparticle decreases. For smaller nanoparticles, it is not obvious how to assign a value of the melting temperature, as the solid–liquid transition occurs over wide range of temperature [37]. We therefore compute the specific heat for the nanoparticles by taking the first derivative of these curves as shown in figure 2. As expected, melting of W bulk produces a sharp peak in the temperature—specific heat curve. For nanoparticles of all different sizes we studied, the heat capacity curves have many peaks over a range of temperatures. For nanoparticles smaller than 8 nm, the specific heat curves fluctuate a lot without a clear distinct peak that can identify a 'melting point'. A distinct peak region starts to emerge only for nanoparticles larger than 8 nm. Thus, we assign the melting point only for nanoparticles larger than 8 nm to the temperature where the maximum peak in the specific heat occurs. The melting temperatures calculated based on the present MD simulation of W nanoparticles are listed in table 3. We note that the melting temperature of bulk W from our MD simulation, 3900 K, is slightly higher than the experimentally measured value of 3695 K [38]. The discrepancy in this result is mainly due to the super-heating of the simulated lattice, as it has been observed that the confined lattice without free surface can be significantly superheated [39, 40]. Although, it is not the main focus of this study, one can follow the procedure prescribed by Morris *et al* [41] to establish co-existence of solid and liquid phases to determine the melting temperature of the bulk W system without super-heating. More importantly, we also note that the melting temperature decreases drastically as the size of the particle decreases. This result suggests that the thermal stability of small nanoparticles must be carefully investigated before they can be used in applications such as nano-devices.

The melting behaviour of 2 nm particle seems to be different from those of bigger particles: at the onset of the melting, the internal energy curve dips down before climbing up again. A similar behaviour has been observed in the melting of small Au nanoparticles of diameters up to 2.8 nm [13]. The onset of melting provides surface atoms an opportunity to rearrange themselves to optimize the local morphology and lower their portion of the internal energy. For extremely small particles, where the surface area to volume ratio is large, this will cause the total internal energy of the particle to decrease briefly as shown in figure 1. The dip and rise in the internal energy indicates a dynamical equilibrium where individual atom passes between solid-like and liquid-like states, such as isomers [42]. Large fluctuations in the heat capacity as shown in figure 2 for nanoparticles smaller than 8 nm give an additional indication that these small particles may undergo the dynamical equilibrium melting regime. However, further study would be needed to elucidate the melting phenomenon in this regime with more certainty.

The variation of the melting temperature with the size of the W nanoparticles is plotted in figure 3. The melting point depression of W nanoparticles exhibit a qualitatively similar behaviour found in the MD simulation of Au nanoparticles [9, 13]. A similar size dependence of melting point depression has been observed experimentally over a broad range of particle sizes for particles in cluster beams [43–46] as well as particles on substrates [6, 7, 47, 48].

For spherical particles of diameter R, a melting temperature $T_m(R)$ can be obtained phenomenologically [4, 5, 49] by equating the Gibbs free energies of solid and liquid

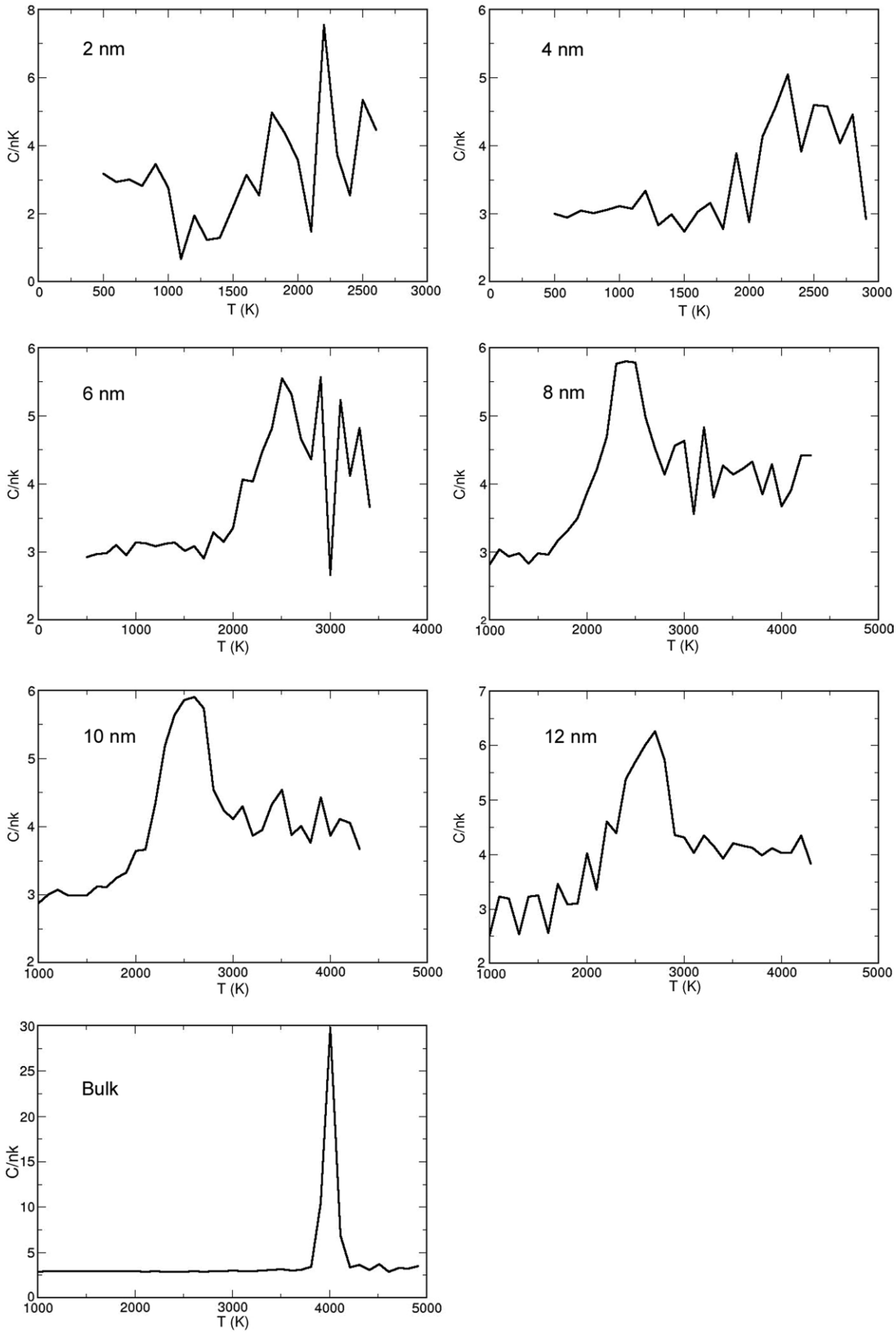

Figure 2. The specific heat per atom of the W nanoparticles with different diameters as a function of temperature. The same data for W bulk are also shown.

spherical clusters, assuming constant pressure conditions:

$$T_{\mathrm{m}}(R) = T^{*}\left(1 - \frac{R_1}{R}\right), \tag{17}$$

where T^{*} is the melting temperature of the bulk tungsten and R_1 is a parameter related to physical quantities such as the solid and liquid densities, the bulk latent heat of melting and solid–vapour and liquid–vapour interface energies. In obtaining this model, the surface energy anisotropy of the solid is not taken into account, and the possibility of inhomogeneous phases (such as a liquid layer due to premelting) is also neglected. The solid line in figure 3 corresponds to the simple thermodynamical model of equation (17) with constant parameter $T^{*} = 3313$ K, and $R_1 = 2.2$ nm. The curve fitting has been done through a standard least squares method.

Table 3. Melting temperatures of W nanoparticles with different diameters.

Diameter (nm)	No of atoms	T_{m} (K)
8.0	16 865	2400
10.0	33 079	2600
12.0	56 905	2700
Bulk	∞	3900

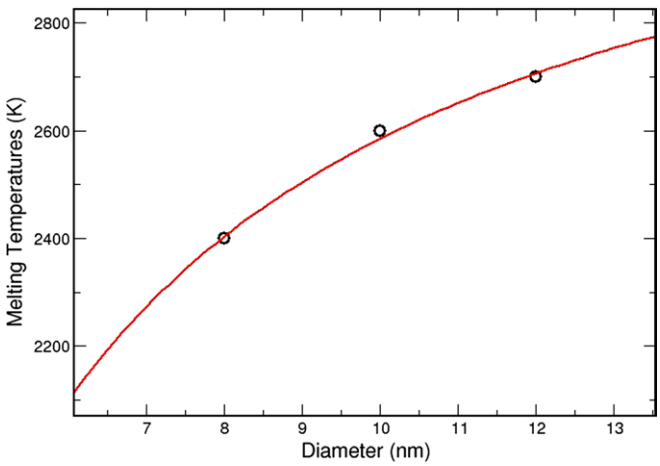

Figure 3. Size dependence of the melting temperatures of W nanoparticles. Symbols represent the calculated values from the present MD simulation and the curves are calculated using equation (17).

The curve in figure 3 shows that the melting point of W nanoparticles decreases according to $1/R$ dependence as predicted in equation (17). However, the fitted value of $T^{*}(3313\ \mathrm{K})$ is significantly lower than the computed melting point of W bulk (3900 K). This is likely related to the tendency of the W interatomic potential used in this study to underestimate several physical properties such as bulk modulus and surface energies (see table 2). Especially, lower surface energies will make nanoparticles that have relatively large surface area to volume ratios to be more susceptible to premelting in the surface layers. This result also indicates that the characteristic of the curve is likely to change for nanoparticles with even larger diameters, and further study with larger nanoparticles will be needed to test the applicability of this model to W nanoparticles using the microscopic indicators, such as Lindemann parameter, the diffusion constant, the principal moment of inertia and the Lipapunov exponents [37].

Hanszen [50] proposed another model of melting in terms of classical thermodynamics assuming that a liquid over-layer forms at the surface of the solid cluster and grows towards the solid core, below the melting point [51, 52]. When the liquid layer thickness exceeds a critical thickness, the whole cluster melts homogeneously. In this model, the melting point $T_{\mathrm{m}}(R)$ of W nanoparticles with diameter R can be expressed as [6, 7]

$$T_{\mathrm{m}}(R) = T^{*}\left(1 - \frac{R_1}{R - t_0} + \frac{R_2}{R}\right). \tag{18}$$

When the data of table 3 were fitted to equation (18), we obtained negligibly small values for t_0 and R_2, thus returning to the model of equation (17).

Figure 4 shows the cross sections of a W nanoparticle with a diameter 10 nm through the centre of the particle at two different temperatures. The colour of each sphere represents the magnitude of the displacement vector that shows how much each atom has moved during the last 6 ps. Figure 4 shows that at a temperature below the melting point the atoms in the entire nanoparticle vibrate in their places while retaining their bcc crystal structure. As the temperature increases, several layers of atoms start to lose their periodicity and form a liquid shell as shown in figure 4(*b*). Once the thickness of the liquid layer reaches a critical thickness, the whole nanoparticle melts.

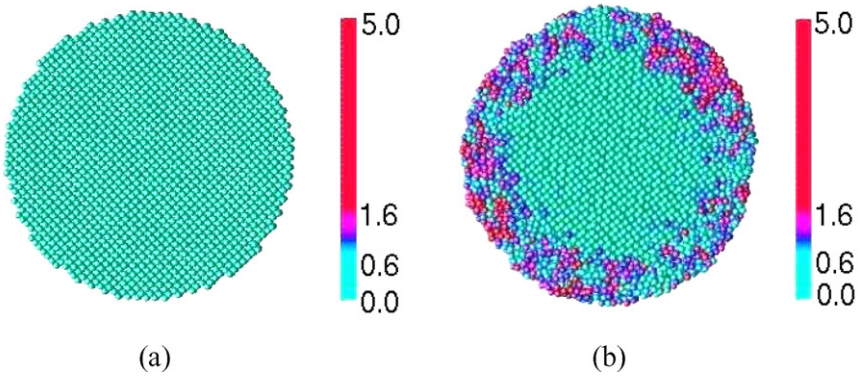

Figure 4. (Colour online) The cross section of W nanoparticle with a diameter 10 nm through the centre of the particle at the temperature of (*a*) 300 K and (*b*) 2000 K. The colour of each sphere represents the magnitude of the displacement vector of each atom during the last 6 ps.

Our MD simulation confirms the experimental observation that nanoscale materials simultaneously display solid-like and liquid-like characteristics, and under thermodynamic equilibrium, a fraction of the atoms in the outer shell of the particle exhibit liquid-like behaviour and the remaining fraction in the inner core acts like solid [7]. Hence, melting point depression and the presence of disorder in nanoscale W powders will play an important role in various industries, including microelectronic industries such as printed circuit board drill bits [53].

5. Conclusions

The thermal stability of unsupported W nanoparticles has been investigated using a MD simulation. The MEAM potential was used to describe the interatomic interactions. Tungsten nanoparticles melt at temperatures that are lower than the bulk melting temperature. The result of our present calculation shows the melting temperature to be approximately a decreasing function of inverse radius. We found that W nanoparticle melting is preceded by surface melting effects of its outer skin, similar to the melting of spherical clusters of many other elements.

Acknowledgments

The authors are grateful to the Center for Advanced Vehicular Systems at Mississippi State University for supporting this study. Computer time allocation has been provided by the High Performance Computing Collaboratory (HPC2) at Mississippi State University.

References

[1] Yih S W H and Wang C T 1979 *Tungsten: Sources, Metallurgy, Properties, and Applications* (New York: Plenum)
[2] Lassner E and Schubert W D 1999 *Tungsten: Properties, Chemistry, Technology of the Element* (New York/New York: Academic/Plenum)
[3] Borel J P 1981 *Surf. Sci.* **106** 1
[4] Gülseren O, Ercolessi F and Tosatti E 1995 *Phys. Rev.* B **51** 7377
[5] Pawlow P 1909 *Z. Phys. Chem.* **65** 545
[6] Lai S L, Guo J Y, Petrova V, Ramanath G and Allen L H 1996 *Phys. Rev. Lett.* **77** 99
[7] Lai S L, Carlsson J R A and Allen L H 1998 *Appl. Phys. Lett.* **72** 1098
[8] Frenken J and Vanderveen J 1985 *Phys. Rev. Lett.* **54** 134
[9] Ercolessi F, Andreoni W and Tosatti E 1991 *Phys. Rev. Lett.* **66** 911
[10] Lewis L J, Jensen P and Barrat J-L 1997 *Phys. Rev.* B **56** 2248
[11] Hall E O 1951 *Proc. Phys. Soc.* B **64** 747
[12] Petch N J 1953 *J. Iron Steel Inst.* 25–8
[13] S J-H, L B-J and C Y W 2002 *Surf. Sci.* **512** 262
[14] Kim S-G and Tománek D 1994 *Phys. Rev. Lett.* **72** 2418
[15] Baskes M I, Nelson J S and Wright A F 1989 *Phys. Rev.* B **40** 6085
[16] Baskes M I 1992 *Phys. Rev.* B **46** 2727
[17] Baskes M I and Johnson R A 1994 *Modelling Simul. Mater. Sci. Eng.* **2** 147
[18] Daw M S 1989 *Phys. Rev.* B **39** 7441
[19] Daw M S and Baskes M I 1984 *Phys. Rev.* B **29** 6443
[20] Daw M S and Baskes M I 1983 *Phys. Rev. Lett.* **50** 1285
[21] Cherne F J, Baskes M I and Deymier P A 2001 *Phys. Rev.* B **65** 024209
[22] Baskes M I, Angelo J E and Bisson C L 1994 *Modelling Simul. Mater. Sci. Eng.* **2** 505
[23] Gall K, Horstemeyer M, Van Schilfgaarde M and Baskes M 2000 *J. Mech. Phys. Solids* **48** 2183
[24] Lee B-J and Baskes M I 2000 *Phys. Rev.* B **62** 8564
[25] Hu W, Zhang B, Huang B, Gao F and Bacon D J 2001 *J. Phys.: Condens. Matter* **13** 1193
[26] Hu W, Deng H, Yuan X and Fukumoto M 2003 *Eur. Phys. J.* B **34** 429
[27] Liu X-Y, Ohotnicky P, Adams J, Rohrer C and Hyland R 1997 *Surf. Sci.* **373** 357
[28] Jelinek B, Houze J, Kim S, Horstemeyer M F, Baskes M I and Kim S-G 2007 *Phys. Rev.* B **75** 054106
[29] Kim Y-M, Lee B-J and Baskes M I 2006 *Phys. Rev.* B **74** 014101
[30] Baskes M I 1997 *Mater. Chem. Phys.* **50** 152
[31] Monkhorst H J and Pack J D 1976 *Phys. Rev.* B **13** 5188
[32] Blöchl P E 1994 *Phys. Rev.* B **50** 17953
[33] Kresse G and Joubert D 1999 *Phys. Rev.* B **59** 1758
[34] Perdew J P, Burke K and Ernzerhof M 1996 *Phys. Rev. Lett.* **77** 3865
[35] Hoover W G 1985 *Phys. Rev.* A **31** 1695
[36] Nosé S 1984 *J. Chem. Phys.* **81** 511
[37] Calvo F and Spiegelmann F 1999 *Phys. Rev. Let.* **82** 2270
[38] Emsley J 1998 *The Elements* 3rd edn (Oxford: Oxford University Press)
[39] Jin Z H and Lu K 1999 *Nanostruct. Mater.* **12** 369
[40] Lu K and Li Y 1998 *Phys. Rev. Lett.* **80** 4474
[41] Morris J R, Wang C Z, Ho K M and Chan C T 1994 *Phys. Rev.* B **49** 3109
[42] Zhao S J, Wang S Q, Cheng D Y and Ye H Q 2001 *J. Phys. Chem.* B **105** 12857
[43] Bertsch G 1997 *Science* **277** 1619
[44] Berry R S 1990 *Sci. Am.* **263** 68
[45] Schmidt M, Kusche R, Von Issendorff B and Haberland H 1998 *Nature* **393** 238
[46] Schmidt M, Kusche R, Kronm Wüller, Von B Issendorff and Haberland H 1997 *Phys. Rev. Lett.* **79** 99
[47] Allen G L, Bayles R A, Gile W W and Jesser W A 1986 *Thin Solid Films* **144** 297
[48] Peters K F, Cohen J B and Chung Y-W 1998 *Phys. Rev.* B **57** 13430
[49] Buffat P and Borel J-P 1976 *Phys. Rev.* A **13** 2287
[50] Hanszen K-J 1960 *Z. Phys.* **157** 523
[51] Efremov M Y, Schiettekatte F, Zhang M, Olson E A, Kwan A T, Berry R S and Allen L H 2000 *Phys. Rev. Lett.* **85** 3560
[52] Zhang M, Efremov M Y, Schiettekatte F, Olson E A, Kwan A T, Lai S L, Wisleder T, Greene J E and Allen L H 2000 *Phys. Rev.* B **62** 10548
[53] Gille G B and Leitner G 2002 *Int. J. Refract. Met. Hard Mater.* **20** 3
[54] Featherstone F H and Neighbours J R 1963 *Phys. Rev.* **130** 1324